Image Registration using Median Absolute Deviation –based Adaptive RANSAC

Khalid Akdim
OPTIMEE Laboratory, Department of Physics, Faculty of Sciences, Moulay Ismail University, Meknes, Morocco
kh.akdim@edu.umi.ac.ma (corresponding author)

Hassane Roukhe
Conception and Systems Laboratory, Department of Physics, Faculty of Sciences, Mohammed V University, Rabat, Morocco
hassane.roukhe@yahoo.fr

Ahmed Roukhe
OPTIMEE Laboratory, Department of Physics, Faculty of Sciences, Moulay Ismail University, Meknes, Morocco
ahmed.roukhe@yahoo.fr

Received: 3 January 2025 | Revised: 2 February 2025 and 15 February 2025 | Accepted: 21 February 2025

 DOI: https://doi.org/10.48084/etasr.10121

ABSTRACT

Image registration encompasses topics such as change detection and remote sensing. Feature-based registration is one of the main approaches and relies on feature extraction and matching. The Oriented FAST and Rotated BRIEF (ORB) algorithm is one of the most robust methods used in feature registration. Random sample consensus (RANSAC) is an optimization method for reducing mismatches in ORB algorithm. However, RANSAC-based methods have certain deficiencies, including rapid increase in computational time, higher false positive ratio, and the need for an empirically determined fixed threshold value. The aforementioned shortcomings result in a reduction in the accuracy of the transform model parameters. In this paper, a modified RANSAC algorithm is proposed, incorporating a Median Absolute Deviation (MAD)-based adaptive threshold, to enhance the efficacy of the method. The threshold value is determined by the MAD of the distances between each point and its model-transformed counterpart. This method enhances the RANSAC algorithm, by taking into consideration the early best matches of each iteration, increasing the number of inliers, and looping through an iterative process based on least squares estimation. The simulation results show that the proposed method is robust to distortion and noise. The results demonstrate that the proposed approach outperforms standard ORB in terms of Mean Squared Error (MSE), Normalized Mutual Information (NMI), Structural Similarity Index Method (SSIM), and Peak Signal-to-Noise Ratio (PSNR).

Keywords-image registration; Oriented FAST and Rotated BRIEF; random sample consensus; MAD; MSE; PSNR; NMI

I. INTRODUCTION

Image registration refers to the process of aligning two or more images of the same scene or object taken from different angles or viewpoints, at different times, or with different sensors [1]. This alignment process enhances interpretability and accuracy in image analysis by finding the optimal geometric transformation that maximizes similarity between reference and sensed images. Image registration is widely applied in remote sensing [2-4]. Image registration methods can generally be divided into two categories: intensity-based [5, 6] and feature-based [7, 8] methods. Intensity-based methods rely on the grayscale distribution of images and use similarity criteria such as mutual information [9] and normalized cross-correlation [10]. While these methods are easy to implement, they face certain challenges. For instance, their performance is poor with images that have significant texture changes [11]. Additionally, the computational complexity of intensity-based methods is high due to the need to process the entire image data [12]. Feature-based approaches extract prominent key points (such as points, corners, edges, etc.), from each image and match them to determine the transformation model. Various comparative studies have shown that feature-based methods outperform other registration approaches [11, 13]. Generally, the feature-based image

registration process consists of four main steps: feature detection, feature matching, transform model estimation, and image resampling [14]. Among these, feature extraction and matching receive more attention due to their crucial roles. A variety of feature point detection approaches have been developed, the most of them based on image gradients. The Oriented FAST and Rotated BRIEF (ORB) algorithm [15] is one of the most efficient methods for detection and matching. It is invariant to rotation changes and stable against variations in illumination, and noise [16]. Despite these advantages, the ORB algorithm has limitations such as the existence of a high error matching rate, scale variance, and reduced performance with complex textures, due to the occurrence of outliers, which affect registration accuracy. Many studies have been conducted on eliminating mismatches [17, 18]. Generally, the existing methods for mismatching removal can be divided into three categories, namely regression-based methods, geometry-based methods, and resampling-based methods [17]. Regression-based methods assume that the correct matches fit a specific model function, with parameters being estimated through regression using feature-point pairs. This approach typically employs the least squares method to minimize error, and mismatches are identified by computing the error in the model. However, this method is sensitive to large errors from mismatches [19]. Geometry-based approaches, such as the Graph Transformation Matching (GTM) [20], combine feature matching with feature geometric properties to construct the topological relationships between the feature points and remove mismatches. However, they struggle with distortions from scale differences and rotation. This may cause the graph of the two images not to be the same. Finally, the resampling-based methods estimate the model that ensures the highest number of matches within a specified error threshold. The most widely used approach in this area is the robust estimation algorithm Random Sample Consensus (RANSAC) [21]. RANSAC is employed to identify mismatches among initial matches and to estimate model transformation parameters. However, this method has certain limitations in scenarios with a high number of outliers and when dealing with nonlinear systems. Consequently, many approaches have been proposed to enhance RANSAC limitations [22]. For instance, the Robust Sample Consensus Judging (RSCJ) algorithm [23] can handle nonlinear transformations and Fast Sample Consensus (FSC) [24] can get more correct matches than RANSAC in a smaller number of iterations, based on the iterative selection of accurate matches. The Maximum Likelihood Estimation Sample Consensus (MLESAC) [25] is a modified version of RANSAC that adds a probability score based on the likelihood that each data point is an inlier, enhancing performance. Progressive Sample Consensus (PROSAC) [26] assumes that some data points have a higher probability of being inliers, which speeds up the sampling probability of hypotheses.

RANSAC uses iterative selection of minimum random samples to estimate model parameters. In other words, the process begins by randomly selecting an initial set of sample points and using them to solve the model parameters Next, it checks the number of inliers and updates the maximum iteration number (N). If the inlier ratio exceeds the value from the previous iteration, N is updated based on the new inlier number. This sequence is continued until the number of iterations reaches the updated N. One major drawback of RANSAC is that during each iteration it only uses the minimum number of points necessary to estimate the model parameters without incorporating new inliers identified in each iteration (or early best matches) to update the model parameters and the possibility to increase the inlier number before moving next iteration. This leaves a considerable number of mismatches (outliers) when the procedure is complete and reduces the registration efficiency. Another disadvantage of RANSAC is that the threshold is empirically chosen. Selection of an optimal threshold value is crucial in RANSAC. In [27, 28], RANSAC is used to eliminate mismatches, but the problem is that the threshold value is manually chosen, which affects the registration accuracy. For example, if a low threshold value is chosen, the rate of correct matches decreases due to the large number of matches being removed as mismatches. In contrast, when selecting a high threshold value, a large number of mismatches are considered correct. Thus, finding an optimal threshold is very important for image registration.

In this paper, a modified RANSAC is proposed. In the proposed method, an iterative process is used in terms of preserving the maximum correct matches obtained in order to improve the performance of the basic RANSAC. Moreover, an adaptive threshold is employed based on the median absolute deviation of the distances between the matching features and their transformed model.

II. ALGORITHM FRAMEWORK

The proposed technique consists of four major steps, as shown in Figure 1: feature extraction using ORB, matching using combination of the cross-checking technique and the K-nearest-neighbor distance criterion, enhanced matching using the proposed adaptive RANSAC algorithm, and transformation model estimation.

III. ORB ALGORITHM

The ORB algorithm is used for feature extraction and description. The algorithm is built upon FAST (Features from Accelerated Segment Test) [29] and BRIEF (Binary Robust Independent Elementary Features) [30]. FAST is used as a feature point detector, and BRIEF is used as a descriptor extractor, each of which will be detailed briefly.

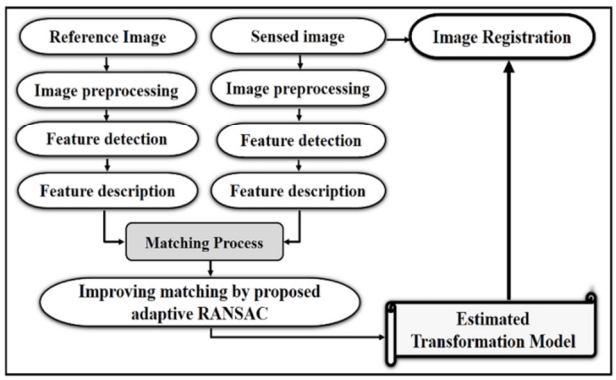

Fig. 1. Flow chart of proposed image registration methodology.

A. Feature Detection

To detect feature points, the ORB algorithm uses the improved FAST method. It first selects a candidate key point in the image and then identifies pixels within a specified radius around this candidate point. If there is a set of continuous neighborhood pixels that are significantly different from the candidate point, then it is identified as a corner point. The steps of detection process are given below:

Step 1: Select a pixel p_x in the image as the center point, with its grayscale value I_{p_x}.

Step 2: select n pixels on a circle with a radius r around the center pointp_x. Typically, r is set to 3 and n is set to 16.

Step 3: Set a threshold intensity value th, then check if there are m continuous pixels, on the cercle, among n pixels whose intensity is greater than $I_{p_x} + th$ or less than$I_{p_x} - th$, consequently I_{p_x} is considered as an interest point.

Step 4: for each pixel in the image, repeat the previous steps.

Step 5: multi-scale image analysis is applied and sampled on each scale level to add a scale invariance to extracted interest points.

Step 6: use intensity centroid method as a measure of feature point orientation to achieve rotation invariance. First, in a patch around a keypoint, the patch moment is defined as:

$$m_{pq} = \sum_{x,y\ in\ patch} x^p y^q\, I(x,y) \quad (1)$$

where $p, q \in \{0,1\}$, x and y represent pixel coordinates, and $I(x,y)$ is the pixel gray value.

The center of mass of the patch can be expressed as:

$$C = \left(\frac{m_{10}}{m_{00}}, \frac{m_{01}}{m_{00}}\right) \quad (2)$$

where m_{00} represents the zero-order moment, while m_{01} and m_{10} denote the first-order moments.

Finally, the orientation of the feature point is determined by:

$$\theta = arctan(\, m_{01}\, / m_{10}) \quad (3)$$

B. Descriptor Extraction

At this step, after detecting keypoints, improved BRIEF [30] is used to calculate the descriptors for each keypoint. BRIEF returns a binary string descriptor that is easy to compute and compare. The descriptor is calculated by selecting a neighborhood area of size $W * W$ around interest point and selecting K_{pt} (usually $K_{pt} = 125$) pairs of pixels in this area by random sampling. Then, a set of binary intensity tests between each pair of pixels is calculated based on (4):

$$\tau(p;u,v) = \begin{cases} 1, & p(u) < p(v) \\ 0, & \text{otherwise} \end{cases} \quad (4)$$

where $p(u)$ and $p(v)$ are the gray value of pair points around the feature point.

Finally, the descriptor of the feature point is expressed as a K_{pt} dimensional vector composed of K_{pt} binary strings according to:

$$f_{\,K}(p) = \sum_{j=1}^{j=K_{pt}} 2^{j-1}\, \tau(p;u_j,v_j) \quad (5)$$

C. Feature Point Matching

The matching task aims to determine the similarity between the descriptors of each feature point in the two images using a distance metric. In this paper, a combination of the cross-checking technique and the K-nearest-neighbor distance ratio is employed to enhance matching accuracy. Cross-checking is a robust technique to ensure the matches between two sets of descriptors are mutual. It works by checking whether the match from the first image to the second image is reciprocated in the opposite direction. The matching process steps are as follows:

Step 1: Cross-checking is initially applied by identifying, for each feature in the first image, the closest match in the second image, and vice versa. During this process, the hamming distance between feature descriptors in both images is computed. Finally, only the mutually consistent matches, where the best match from the first image to the second image corresponds to the same feature when matched in the opposite direction, are retained.

Step 2: After the cross-check, the K-nearest-neighbor distance ratio is used (K = 2) according to [31]:

$$\left\| \frac{D_{f_i} - D_{f_c}}{D_{f_i} - D_{f_s}} \right\| < T_r \quad (6)$$

where D_{f_c} is the closest neighbor's descriptor to the descriptor D_{f_i}, and D_{f_s} is the second closest neighbor's descriptor to D_{f_i}. If this ratio is smaller than the threshold value T_r, the match is considered valid. The value of T_r is set to 0.85 [32]. This contributes to discarding ambiguous matches where the best and the second-best are too similar.

IV. IMPROVING MATCHING WITH THE PROPOSED RANSAC

In this section, the standard RANSAC is introduced. Following that, the proposed Adaptive RANSAC is presented in detail.

A. Standard RANSAC

It is important to understand how the RANSAC-based algorithm works in order to understand the improvements we propose. RANSAC is an iterative method for identifying correct matches from a set of observed data containing outliers. The algorithm is applicable in the estimation of the parameters of a mathematical model. In the first step, a suitable model is selected according to the transformation model according to the nature of the images and geometric relationship. In order to estimate the parameters of the model, a necessary number of matched points n_s, is randomly selected and calculated based on (7):

$$n_s = \frac{p}{2} \quad (7)$$

where p is the number of parameters in the transformation model.

For example, in similarity transform that needs four parameters, two matching points must be selected, to estimate the transformation parameters according to (8):

$$\begin{bmatrix} X_1' \\ Y_1' \\ X_2' \\ Y_2' \end{bmatrix} = \begin{bmatrix} X_1 & -Y_1 & 1 & 0 \\ Y_1 & X_1 & 0 & 1 \\ X_2 & -Y_2 & 1 & 0 \\ Y_2 & X_2 & 0 & 1 \end{bmatrix} \begin{bmatrix} a \\ b \\ c \\ d \end{bmatrix} \quad (8)$$

where (X_1', Y_1') and (X_2', Y_2') are the coordinates of the matching points in the reference image, while (X_1, Y_1), (X_2, Y_2) are the matching point coordinates in the sensed image, and a, $b, c,$ and d represent the model parameters.

In the second step, after computing the transformation model parameters, the model M is tested by calculating the Euclidean distance between each matching point in the reference image and its transformed model in the sensed image to determine the number of inliers at each iteration (I_{iter}), the inlier ratio (w), and the number of iterations (N_{MAX}) using (9) and (10). If this distance is less than a preset threshold, this point correspondence is considered valid, otherwise it is discarded. The inlier ratio can be explained as the probability of selecting an inlier each time a single point is chosen; in other words, it is the ratio between the number of inliers and the total number of dataset(N).

$$1 - (1 - w^{n_s})^{N_{MAX}} = P_{rob} \quad (9)$$

$$w = \frac{I_{iter}}{N} \quad (10)$$

where P_{rob} is the desired probability of choosing at least one sample free from outliers.

In the subsequent iteration, if I_{iter} is greater than the previous value, N_{MAX} is updated using the newI_{iter}; otherwise, N_{MAX} remains the same. This process continues until the iteration count reaches N_{MAX} or the inlier ratio (w) exceeds a specified threshold. It is important to highlight that N_{MAX} is an adaptive termination criterion that is adjusted in each iteration according to w. Finally, the subset with the largest number of inliers is regarded as the most accurate matching points, while the model formed with these inliers is considered the optimal one. Figure 2 shows the flowchart of Standard RANSAC.

A. The Proposed Adaptive RANSAC

As stated earlier, RANSAC estimates the model parameters using an initial random sample of the minimum number of matched points and then evaluates the model against all additional matched points to identify inliers. If the number of inliers discovered in each iteration exceeds the previous count, the current best inliers are updated. However, the algorithm does not use these initial inliers to refine the model. Therefore, an iterative process is introduced to incorporate the best matches (inliers) found in each iteration. The proposed method involves a loop where all inliers identified during each iteration are directly used to estimate the model's unknown parameters, which are calculated using the least squares method. Unlike RANSAC, which updates the model based on a minimal subset of points in each iteration, this approach utilizes all inliers found during each iteration and applies a least squares solution to refine the model. After each internal iteration, the adaptive criterion is adjusted based on the maximum number of inliers detected in the local loop. Moreover, in this modified variant of RANSAC, to remove mismatches and improve the registration process during the model testing step, a median absolute deviation-based adaptive threshold and distance function are suggested. Figure 3 shows the flowchart of modified RANSAC. The details of the adaptive threshold, distance function, and the pseudocode for the iterative process are described below.

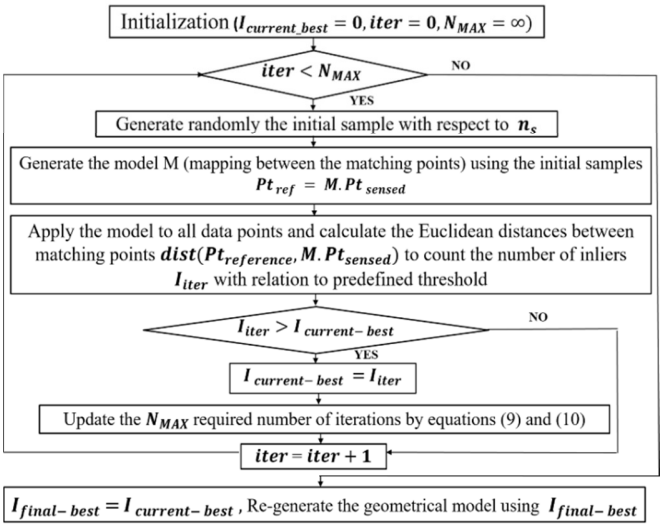

Fig. 2. Flowchart of the standard RANSAC.

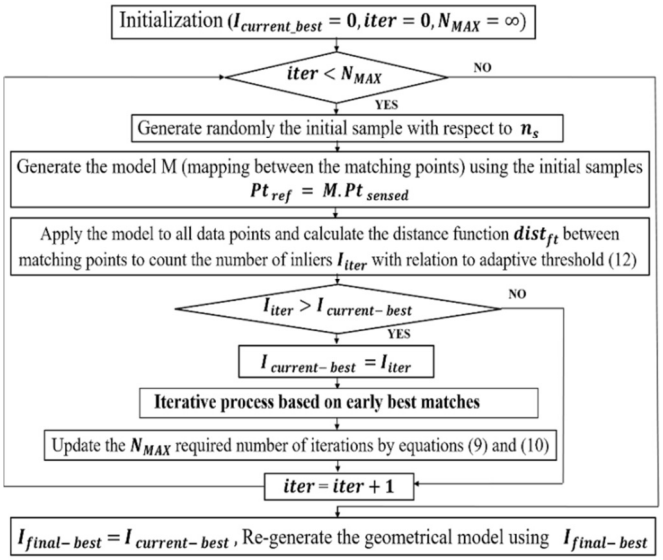

Fig. 3. Flowchart of the modified RANSAC.

1) Median Absolute Deviation-based Adaptive Threshold

In this approach, the distance between Pt_{ref} and its corresponding transformed model $M * Pt_{sensed}$ is first calculated for all matching points in the reference image and their transformed model in the sensed image following to (11).

Then, according to (12), the Median Absolute Deviation (MAD) of these distances is used as the threshold. Afterward, the model is tested through a distance function $dist_{ft}$, for each corresponding point in the reference image and its transformed model in the sensed image, the distance function $dist_{ft}$ is computed as shown in (13). If this distance function is less than the adaptive threshold, the correspondence is considered valid, otherwise, the point is marked as a mismatch and is subsequently removed from both the reference and sensed images [33].

$$d_j = dist = \left\| Pt_{ref_j} - M * Pt_{sensed_j} \right\|_2 \quad (11)$$

for every j in $[0, m-1]$.

$$MAD = \beta * med_{\,0\le j\le m-1} \left| d_j - med_{\,0\le i\le M-1}(d_i) \right| \quad (12)$$

$$dist_{ft} = \frac{|d_j - med_{\,0\le i\le m-1}(d_i)|}{c} \quad (13)$$

where m is the number of matching points, Pt_{ref_j} is the jth match in the reference image, $M * Pt_{sensed_j}$ is the jth reference model of matching transformation in the sensed image, β is a scale constant that makes the MAD consistent (β is set to 1.4826) [34], med represents the median of distances, c is a standard score demonstrating how far a data point is from the average of a dataset (in this paper, c is set to 3), and $\|.\|_2$ is the Euclidean norm.

2) Iterative Process Pseudocode

The psoeudocode steps of the iterative process are shown below:

Inputs:
- $I_{current-best}$: the number of the best inliers after comparing with the ones of previous iteration
- m: the size of all matching points
Output:
I_{final_best}: Best-inliers
Variables:
- $I_{save\_best} = 0$
- $Th_{adapt} = 0$, Th_{adapt} denotes the adaptive threshold, initialized by zero
- $I_{loop\_best} = 0$
While ($I_{loop\_best} > I_{current-best}$ OR $I_{loop\_best} = 0$) do
  If $I_{loop\_best} \neq 0$ then
    $I_{current-best} = I_{loop\_best}$
  End If
  Select all inliers ($I_{current-best}$) as the new initial sample.
  Generate a new least-squares-based transformation model using this new sample
  Compute the adaptive threshold Th_{adapt}
  Evaluate the model against all matching points (m) using the distance function $dist_{ft}$ and the adaptive threshold 12)
  Count the number of data points (I_{loop_best})
End While
If $I_{current-best} \geq I_{save\_best}$ then
  $I_{save\_best} = I_{current-best}$
Else
  $I_{current-best} = I_{save\_best}$
End If
$I_{final\_best} = I_{current-best}$

V. EXPERIMENTAL RESULTS

In this part, the performance of the proposed method is evaluated in three images with different texture conditions and modalities. To investigate the effectiveness of the proposed method, it is compared with the standard ORB matching [15]. The experiments were executed on a PC with a 2.3Ghz Intel Core i5, 8Go RAM memory, implemented in Python 3.9.

A. Dataset

Several experiments are conducted to assess the validity of the proposed technique. First, a set of tests is examined on images with different angles. Then, a set of experiments against scale changes is tested. Third, the key point number effect is evaluated. Then, the images are artificially infected by Gaussian noise. Finally, the performance of the proposed method in the matching process is evaluated. Figure 4 depicts the images of the dataset used and were taken from [35-37]. The images used are in jpeg format.

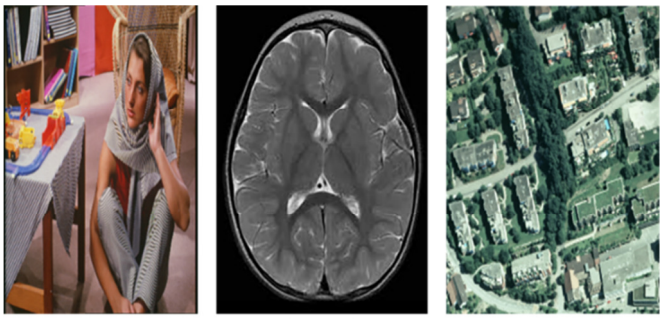

(a) (b) (c)

Fig. 4. Test images: (a) Barbara [35], (b) Brain scan [36], (c) Zurich Hoengg [37].

B. Performance Metrics

The effectiveness of the proposed method is evaluated based on the two categories of quantitative criteria. The first is the registration criteria, including the Mean Square Error (MSE) [38] according to (14), the Peak Signal-to-Noise Ratio (PSNR) [39] according to (15), the Normalized Mutual Information NMI [40] according to (16), and the Structural Similarity Index Measure (SSIM) [41, 42] according to (17). The second category is the matching criteria, including the precision (P_r) according to (18), the False Positive Ratio (FPR) according to (19), the Sum of Inverse Total Number of Matching and Mismatch Ratio (SITMMR) [43] according to (20), and the Subtraction of Inverse Total Number of Matching and Matching Correctness (SITMMC) [43] according to (21):

$$\text{MSE} = \frac{1}{L*W}\sum_{i=0}^{i=L-1}\sum_{j=0}^{j=W-1}\left(I(i,j)-J(i,j)\right)^2 \quad (14)$$

$$\text{PSNR} = 20\,log_{10}\left[\frac{255}{\sqrt{MSE}}\right] \quad (15)$$

$$\text{NMI}(I,J) = \frac{H(I)+H(J)}{H(I,J)} \quad (16)$$

where $H(I)$ and $H(J)$ denote the entropy values of I and J respectively. H is defined as: $H(I) = -\sum_{i=0}^{i=DYN-1} p_i \log_2(p_i)$, while $H(I,J)$ represents their joint entropy, and p_i is the probability of a pixel having gray level i.

$$\text{SSIM}(I,J) = \frac{(2\,u_I u_J + c_1)(2\,\delta_{IJ} + c_2)}{(u_I^2 + u_J^2 + c_1)(\delta_I^2 + \delta_J^2 + c_2)} \quad (17)$$

$$P_r = \frac{N_{TM}}{N_{TM}+N_{FM}} \quad (18)$$

$$\text{FPR} = \frac{N_{FM}}{N_{TM}+N_{FM}} \quad (19)$$

$$\text{SITMMR} = \frac{N_{FM}+1}{N_{TM}+N_{FM}} \quad (20)$$

$$\text{SITMMC} = \frac{N_{TM}-1}{N_{TM}+N_{FM}} \quad (21)$$

In the above, the images being compared are denoted by I and J, and (L,W) is their size. DYN refers to the dynamic range of the image, in (17), u and δ represent the mean value and the dispersion, c_1 and c_2 are constants used to stabilize the division when the denominator is close to zero, and N_{FM} and N_{TM} are the numbers of true matches number and mismatches.

C. Scale effect

To evaluate the influence of scale variation, the images of Figure 4, are used. A scale variation from 0.5 to 2 with a scale factor of 0.25 was applied to the sensed images. Figure 5 displays the average precision matching of the proposed method compared to ORB under scale change. The proposed method has better performance and more stability against scale changes compared to ORB. If the scale factor between the image pairs is above two, the proposed approach fails in image registration.

D. Angle Effect

In this experiment, to assess the effectiveness of the proposed method against image rotation, image (a) and image (b) from Figure 4 were used, and the sensed images were rotated from 5° to 65° with 10° steps, whereas the reference images and scale were kept fixed. Table I presents the registration performance metrics in comparison to standard ORB for image (a). It can be seen from the experimental results that the proposed method registers images with different angle better than standard ORB in terms of MSE, PSNR, NMI, and SSIM, while Table II shows the estimated angle and scale for the same image, in comparison to standard ORB, relative to the actual angle. The obtained results demonstrate that the proposed method outperforms the standard ORB in estimating actual angle and maintaining a fixed scale. Figures 6 and 7 illustrate two examples of the registration results and the graphical representation of the performance metrics (MSE, PSNR, NMI, SSIM) respectively for image (b) using both methods.

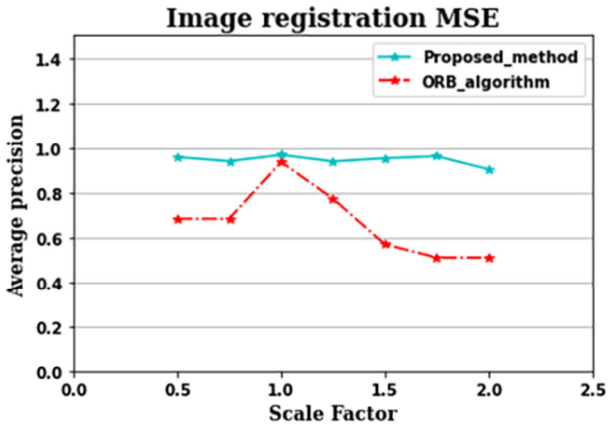

Fig. 5. Average precision relative to scale change by proposed method and ORB.

E. Testing with Noise

In this experiment, Gaussian noise was applied to all considered images. Multiple variance levels, ranging from 0.02 to 0.09, were progressively applied to each sensed image, along with a rotation of 25° and a scale change of 1.2. Figure 8 shows a visual result of registering the image (c) corrupted by Gaussian noise with a variance of 0.07. Table III compares the performance of the proposed method to that of ORB. The results prove the superiority of proposed method, consistently providing higher PSNR, NMI, and SSIM values, and lower MSE value.

TABLE I. COMPARISON OF ESTIMATED ANGLES AND SCALES AGAINST TRUE ANGLES FOR IMAGE (a) IN COMPARISON TO STANDARD ORB

Angle (deg)	**ORB [15]**				**Proposed**			
	Estimated angle	***Estimated scale***	***Angle error***	***Scale error***	***Estimated angle***	***Estimated scale***	***Angle error***	***Scale error***
05	5.137	0.974	0.137	0.025	5.011	0.999	0.0112	0.0003
15	15.177	0.956	0.179	0.044	15.003	1.001	0.0032	0.0004
25	25.270	0.963	0.270	0.037	25.016	1.001	0.0156	0.0001
35	35.042	0.959	0.042	0.041	35.019	0.9999	0.0189	0.0001
45	45.112	0.971	0.112	0.029	45.015	0.9999	0.0150	0.0001
55	55.345	0.952	0.345	0.048	55.027	0.9999	0.0268	0.0001
65	64.821	0.975	0.179	0.025	65.019	1.0003	0.0199	0.0003

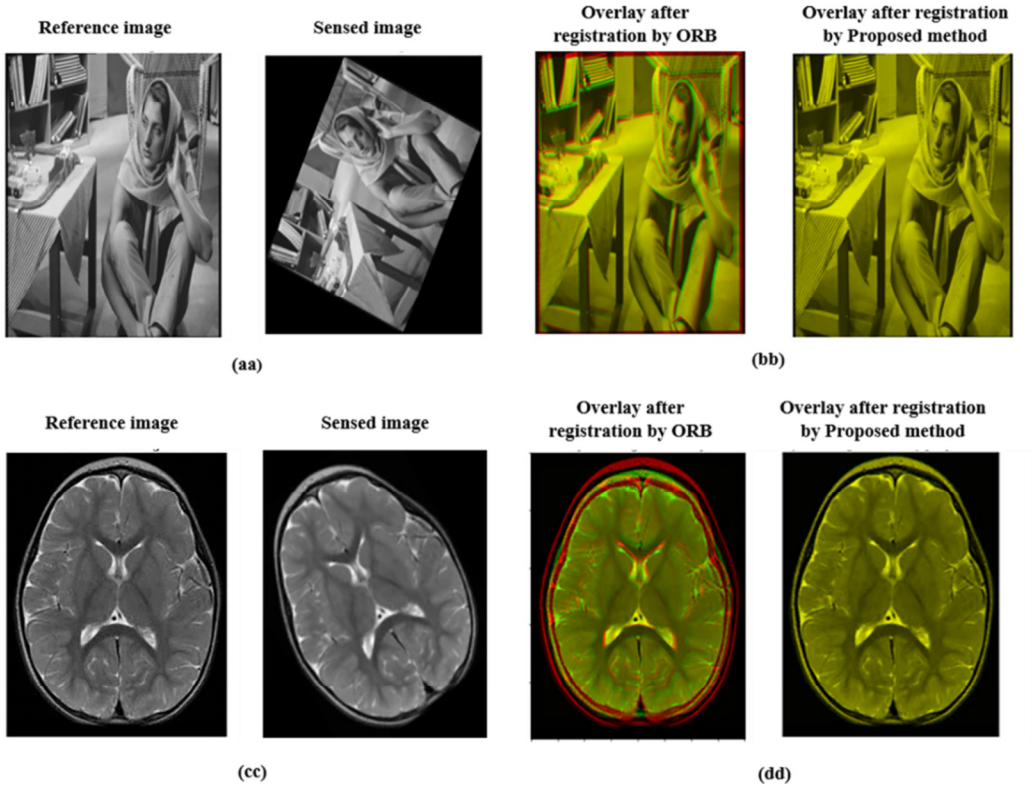

Fig. 6. Rotation variation results in image registration. (aa) Reference and sensed (a) images with 65◦rotation angle. (bb) Registration result of the ORB and the proposed method for image (a). (cc) Reference and sensed (b) images with 35◦rotation angle. (dd) Registration result of the ORB and proposed method.

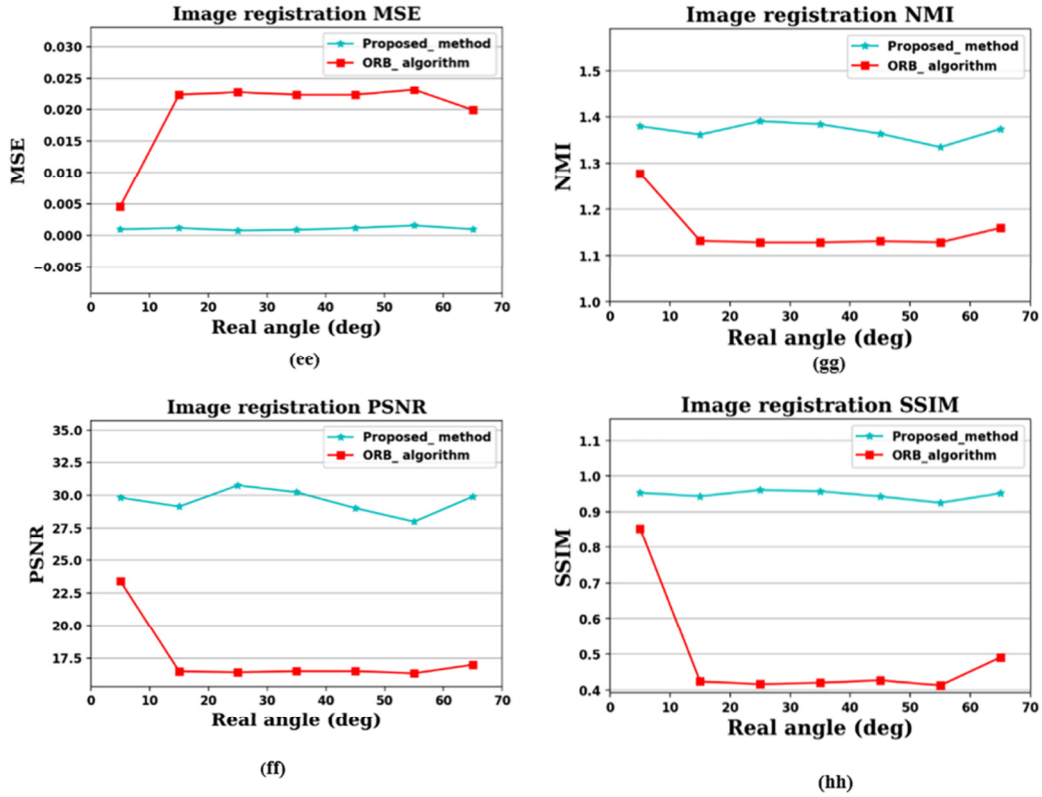

Fig. 7. Registration criteria graphs for image (b).

TABLE II. MSE, PSNR, NMI, AND SSIM VALUE COMPARISON WITH RESPECT TO NOISE LEVELS

Image	Noise variance		0.02	0.03	0.04	0.05	0.06	0.07	0.08	0.09
Image (a)	ORB [15]	MSE	0.0092	0.0200	0.0222	0.0193	0.0252	0.0508	0.0258	0.0292
		PSNR	20.3781	16.9838	16.5194	17.1433	15.9800	12.9378	15.8789	15.3483
		NMI	1.0967	1.0584	1.0532	1.05433	1.0426	1.0147	1.0398	1.0370
		SSIM	0.3741	0.1784	0.1423	0.1712	0.1168	0.0409	0.1225	0.0986
	Proposed	MSE	**0.0064**	**0.0109**	**0.0143**	**0.0141**	**0.0172**	**0.0218**	**0.01979**	**0.0195**
		PSNR	**21.9432**	**19.6317**	**18.4342**	**18.4813**	**17.6525**	**16.620**	**17.0340**	**17.0874**
		NMI	**1.1164**	**1.0858**	**1.0704**	**1.0692**	**1.0585**	**1.0468**	**1.0517**	**1.0519**
		SSIM	**0.4723**	**0.34204**	**0.2562**	**0.2885**	**0.2638**	**0.1586**	**0.2197**	**0.2515**
Image (b)	ORB [15]	MSE	0.0287	0.0345	0.0621	0.0520	0.0260	0.0297	0.0547	0.0383
		PSNR	15.4239	14.6251	12.0677	12.8387	15.8511	15.2665	12.6209	14.1682
		NMI	1.0821	1.0790	1.0679	1.0735	1.0655	1.0538	1.0719	1.0414
		SSIM	0.1499	0.1484	0.1542	0.1484	0.1091	0.1023	0.1457	0.0612
	Proposed	MSE	**0.0065**	**0.0094**	**0.0111**	**0.0154**	**0.0157**	**0.0211**	**0.0210**	**0.0289**
		PSNR	**21.8319**	**20.2651**	**19.5380**	**18.1190**	**18.0419**	**16.7556**	**16.7817**	**15.3784**
		NMI	**1.1287**	**1.1088**	**1.0987**	**1.0831**	**1.0805**	**1.0668**	**1.0667**	**1.0524**
		SSIM	**0.4104**	**0.3422**	**0.3174**	**0.2482**	**0.2587**	**0.1918**	**0.1939**	**0.1158**
Image (c)	ORB [15]	MSE	0.0606	0.0854	0.1056	0.1385	0.1173	0.1623	0.1680	0.1359
		PSNR	12.1748	10.6845	9.7628	8.5837	9.3064	7.8962	7.7456	8.6675
		NMI	0.0982	1.0167	1.0090	1.0049	1.0064	1.0045	1.0034	1.0045
		SSIM	0.0606	0.0503	0.0409	0.0254	0.0312	0.0246	0.0181	0.0216
	Proposed	MSE	**0.0057**	**0.0079**	**0.0100**	**0.0117**	**0.0131**	**0.0150**	**0.0166**	**0.0185**
		PSNR	**22.4589**	**21.0330**	**19.9821**	**19.306**	**18.8117**	**18.2437**	**17.8046**	**17.3158**
		NMI	**1.1518**	**1.1288**	**1.1128**	**1.1027**	**1.0954**	**1.0875**	**1.0814**	**1.0750**
		SSIM	**0.6040**	**0.5355**	**0.4843**	**0.4535**	**0.4317**	**0.4038**	**0.3843**	**0.3620**

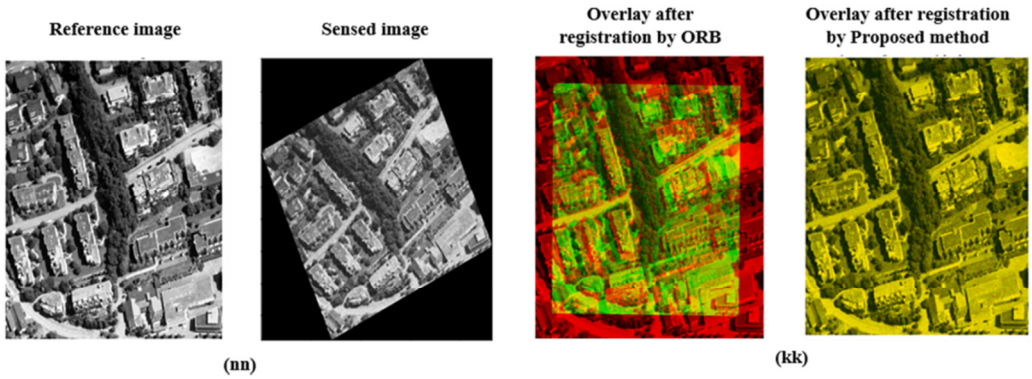

Fig.8. Image registration results for image (c) with gaussian noise of 0.07 variance, rotation of 25° and scale of 1.2. (nn) Reference and sensed image for image (c). (kk) Registration results for image (c).

F. Evaluation of the Proposed Method's Performance in the Matching Process

In this experiment, to evaluate the performance of the proposed method in the matching process, a pair of (c) images from Figure 4 with different viewpoints and scale was used. The results can be seen in Table IV. The precision (P_r), and SITMMC of the proposed method have higher values, whereas the FPR and SITMMR have lower. Furthermore, the proposed approach can remove higher number of mismatches while preserving more accurate matches.

TABLE III. RESULTS OF MATCHING PROCESS

Method	P_r	FPR	SITMMR	SITMMC	NTM	NFM
ORB [15]	0.668	0.332	0.336	0.663	141	70
Proposed	0.936	0.064	0.071	0.929	132	9

VI. CONCLUSION

In this paper, an adaptive RANSAC–based method was presented for improving the performance of the image registration process by removing a significant number of mismatches between images, selecting an appropriate threshold value, preserving more correct matches, and enhancing the matching precision and registration accuracy.

The proposed method is based on feature extraction by the ORB algorithm and matching through cross-checking combined with the K-nearest-neighbor distance ratio. Our contribution lies in improving the matching process performance by using an adaptive RANSAC algorithm. A local iterative process is introduced to increase the number of inliers along with a MAD-based adaptive threshold with a distance function for optimal choosing of threshold value in the RANSAC. To evaluate the efficiency of the proposed approach, various transformations such as scaling, rotation, and noise were applied to the original considered images. The proposed approach was tested based on matching evaluation and registration criteria. The experimental results show that the suggested method has outstanding performance compared to standard ORB.

REFERENCES

[1] L. G. Brown, "A survey of image registration techniques," *ACM Computing Surveys*, vol. 24, no. 4, pp. 325–376, Sep. 1992, https://doi.org/10.1145/146370.146374.

[2] R. Vadhi, V. S. Kilari, and S. S. Kumar, "An Image Fusion Technique Based on Hadamard Transform and HVS," *Engineering, Technology & Applied Science Research*, vol. 6, no. 4, pp. 1075–1079, Aug. 2016, https://doi.org/10.48084/etasr.707.

[3] C.-L. Tsai, C.-Y. Li, G. Yang, and K.-S. Lin, "The Edge-Driven Dual-Bootstrap Iterative Closest Point Algorithm for Registration of Multimodal Fluorescein Angiogram Sequence," *IEEE Transactions on Medical Imaging*, vol. 29, no. 3, pp. 636–649, Mar. 2010, https://doi.org/10.1109/TMI.2009.2030324.

[4] S. Singh *et al.*, "A review of image fusion: Methods, applications and performance metrics," *Digital Signal Processing*, vol. 137, Jun. 2023, Art. no. 104020, https://doi.org/10.1016/j.dsp.2023.104020.

[5] J. Kim and J. A. Fessler, "Intensity-based image registration using robust correlation coefficients," *IEEE Transactions on Medical Imaging*, vol. 23, no. 11, pp. 1430–1444, Aug. 2004, https://doi.org/10.1109/TMI.2004.835313.

[6] A. Goshtasby, G. C. Stockman, and C. V. Page, "A Region-Based Approach to Digital Image Registration with Subpixel Accuracy," *IEEE Transactions on Geoscience and Remote Sensing*, vol. GE-24, no. 3, pp. 390–399, Feb. 1986, https://doi.org/10.1109/TGRS.1986.289597.

[7] J. Zheng, J. Tian, K. Deng, X. Dai, X. Zhang, and M. Xu, "Salient Feature Region: A New Method for Retinal Image Registration," *IEEE Transactions on Information Technology in Biomedicine*, vol. 15, no. 2, pp. 221–232, Mar. 2011, https://doi.org/10.1109/TITB.2010.2091145.

[8] S.-Y. Guan, T.-M. Wang, C. Meng, and J.-C. Wang, "A Review of Point Feature Based Medical Image Registration," *Chinese Journal of Mechanical Engineering*, vol. 31, no. 1, Aug. 2018, Art. no. 76, https://doi.org/10.1186/s10033-018-0275-9.

[9] H. Chen, "Mutual Information: A Similarity Measure for Intensity Based Image Registration," in *Advanced Image Processing Techniques for Remotely Sensed Hyperspectral Data*, P. K. Varshney and M. K. Arora, Eds. New York, NY, USA: Springer, 2004, pp. 89–108.

[10] M. Debella-Gilo and A. Kaab, "Sub-pixel precision image matching for measuring surface displacements on mass movements using normalized cross-correlation," *Remote Sensing of Environment*, vol. 115, no. 1, pp. 130–142, Jan. 2011, https://doi.org/10.1016/j.rse.2010.08.012.

[11] G. Sreeja and O. Saraniya, "A Comparative Study on Image Registration Techniques for SAR Images," in *5th International Conference on Advanced Computing & Communication Systems*, Coimbatore, India, Mar. 2019, pp. 947–953, https://doi.org/10.1109/ICACCS.2019.8728390.

[12] D. Zhang, H. Wei, X. Huang, and H. Ni, "Research on high precision image registration method based on line segment feature and ICP algorithm," in *International Conference on Optics and Machine Vision*, Changsha, China, Jan. 2023, vol. 12634, pp. 90–96, https://doi.org/10.1117/12.2678654.

[13] S. Dawn, V. Saxena, and B. Sharma, "Remote Sensing Image Registration Techniques: A Survey," in *International Conference on Image and Signal Processing*, Trois-Rivieres, QC, Canada, Jul. 2010, pp. 103–112, https://doi.org/10.1007/978-3-642-13681-8_13.

[14] B. Zitova and J. Flusser, "Image registration methods: a survey," *Image and Vision Computing*, vol. 21, no. 11, pp. 977–1000, Oct. 2003, https://doi.org/10.1016/S0262-8856(03)00137-9.

[15] E. Rublee, V. Rabaud, K. Konolige, and G. Bradski, "ORB: An efficient alternative to SIFT or SURF," in *International Conference on Computer Vision*, Barcelona, Spain, Nov. 2011, pp. 2564–2571, https://doi.org/10.1109/ICCV.2011.6126544.

[16] Y. Dai and J. Wu, "An Improved ORB Feature Extraction Algorithm Based on Enhanced Image and Truncated Adaptive Threshold," *IEEE Access*, vol. 11, pp. 32073–32081, Jan. 2023, https://doi.org/10.1109/ACCESS.2023.3261665.

[17] Z. He, C. Shen, Q. Wang, X. Zhao, and H. Jiang, "Mismatching Removal for Feature-Point Matching Based on Triangular Topology Probability Sampling Consensus," *Remote Sensing*, vol. 14, no. 3, Jan. 2022, Art. no. 706, https://doi.org/10.3390/rs14030706.

[18] J. Ma, J. Zhao, J. Tian, X. Bai, and Z. Tu, "Regularized vector field learning with sparse approximation for mismatch removal," *Pattern Recognition*, vol. 46, no. 12, pp. 3519–3532, Dec. 2013, https://doi.org/10.1016/j.patcog.2013.05.017.

[19] G. Wang, Z. Wang, Y. Chen, Q. Zhou, and W. Zhao, "Removing mismatches for retinal image registration via multi-attribute-driven regularized mixture model," *Information Sciences*, vol. 372, pp. 492–504, Dec. 2016, https://doi.org/10.1016/j.ins.2016.08.041.

[20] W. Aguilar, Y. Frauel, F. Escolano, M. E. Martinez-Perez, A. Espinosa-Romero, and M. A. Lozano, "A robust Graph Transformation Matching for non-rigid registration," *Image and Vision Computing*, vol. 27, no. 7, pp. 897–910, Jun. 2009, https://doi.org/10.1016/j.imavis.2008.05.004.

[21] M. A. Fischler and R. C. Bolles, "Random sample consensus: a paradigm for model fitting with applications to image analysis and automated cartography," *Communications of the ACM*, vol. 24, no. 6, pp. 381–395, Mar. 1981, https://doi.org/10.1145/358669.358692.

[22] B. Salehi, S. Jarahizadeh, and A. Sarafraz, "An Improved RANSAC Outlier Rejection Method for UAV-Derived Point Cloud," *Remote Sensing*, vol. 14, no. 19, Jan. 2022, Art. no. 4917, https://doi.org/10.3390/rs14194917.

[23] B. Li and H. Ye, "RSCJ: Robust Sample Consensus Judging Algorithm for Remote Sensing Image Registration," *IEEE Geoscience and Remote Sensing Letters*, vol. 9, no. 4, pp. 574–578, Jul. 2012, https://doi.org/10.1109/LGRS.2011.2175434.

[24] Y. Wu, W. Ma, M. Gong, L. Su, and L. Jiao, "A Novel Point-Matching Algorithm Based on Fast Sample Consensus for Image Registration," *IEEE Geoscience and Remote Sensing Letters*, vol. 12, no. 1, pp. 43–47, Jan. 2015, https://doi.org/10.1109/LGRS.2014.2325970.

[25] P. H. S. Torr and A. Zisserman, "MLESAC: A New Robust Estimator with Application to Estimating Image Geometry," *Computer Vision and Image Understanding*, vol. 78, no. 1, pp. 138–156, Apr. 2000, https://doi.org/10.1006/cviu.1999.0832.

[26] O. Chum and J. Matas, "Matching with PROSAC - progressive sample consensus," in *Computer Society Conference on Computer Vision and Pattern Recognition*, San Diego, CA, USA, Jun. 2005, vol. 1, pp. 220–226, https://doi.org/10.1109/CVPR.2005.221.

[27] Y. Ye and J. Shan, "A local descriptor based registration method for multispectral remote sensing images with non-linear intensity differences," *ISPRS Journal of Photogrammetry and Remote Sensing*, vol. 90, pp. 83–95, Apr. 2014, https://doi.org/10.1016/j.isprsjprs.2014.01.009.

[28] F. Guo, X. Zhao, B. Zou, and Y. Liang, "Automatic Retinal Image Registration Using Blood Vessel Segmentation and SIFT Feature," *International Journal of Pattern Recognition and Artificial Intelligence*, vol. 31, no. 11, Nov. 2017, Art. no. 1757006, https://doi.org/10.1142/S0218001417570063.

[29] E. Rosten and T. Drummond, "Machine Learning for High-Speed Corner Detection," in *European Conference on Computer Vision*, Graz, Austria, Dec. 2006, pp. 430–443, https://doi.org/10.1007/11744023_34.

[30] M. Calonder, V. Lepetit, C. Strecha, and P. Fua, "BRIEF: Binary Robust Independent Elementary Features," in *European Conference on Computer Vision*, Heraklion, Greece, Sep. 2010, pp. 778–792, https://doi.org/10.1007/978-3-642-15561-1_56.

[31] H. Yan, G. Lv, X. Ren, and X. Dong, "Improved Nearest Neighbor Distance Ratio for Matching Local Image Descriptors," in *International CCF Conference on Artificial Intelligence*, Jinan, China, Aug. 2018, pp. 185–197, https://doi.org/10.1007/978-981-13-2122-1_14.

[32] D. G. Lowe, "Object recognition from local scale-invariant features," in *Seventh IEEE International Conference on Computer Vision*, Kerkyra, Greece, Sep. 1999, vol. 2, pp. 1150–1157 vol.2, https://doi.org/10.1109/ICCV.1999.790410.

[33] C. Croux and P. J. Rousseeuw, "Time-Efficient Algorithms for Two Highly Robust Estimators of Scale," in *Computational Statistics*, Y. Dodge and J. Whittaker, Eds. Heidelberg, Germany: Physica-Verlag, 1992, pp. 411–428.

[34] P. J. Rousseeuw and M. Hubert, "Anomaly detection by robust statistics," *WIREs Data Mining and Knowledge Discovery*, vol. 8, no. 2, 2018, Art. no. e1236, https://doi.org/10.1002/widm.1236.

[35] "Enc_Dec_Times." https://kaggle.com/code/kenny3s/enc-dec-times.

[36] "Brain MRI Images for Brain Tumor Detection." https://www.kaggle.com/datasets/navoneel/brain-mri-images-for-brain-tumor-detection.

[37] "ISPRS Data sets: Zurich Hoengg." https://www.isprs.org/resources/datasets/sample-datasets/hoengg/cutouts.aspx.

[38] J. Sogaard *et al.*, "Applicability of Existing Objective Metrics of Perceptual Quality for Adaptive Video Streaming," *Electronic Imaging*, vol. 28, pp. 1–7, Feb. 2016, https://doi.org/10.2352/ISSN.2470-1173.2016.13.IQSP-206.

[39] S. Rani, Y. Chabrra, and K. Malik, "An Improved Denoising Algorithm for Removing Noise in Color Images," *Engineering, Technology & Applied Science Research*, vol. 12, no. 3, pp. 8738–8744, Jun. 2022, https://doi.org/10.48084/etasr.4952.

[40] C. Studholme, D. L. G. Hill, and D. J. Hawkes, "An overlap invariant entropy measure of 3D medical image alignment," *Pattern Recognition*, vol. 32, no. 1, pp. 71–86, Jan. 1999, https://doi.org/10.1016/S0031-3203(98)00091-0.

[41] U. Sara, M. Akter, and M. S. Uddin, "Image Quality Assessment through FSIM, SSIM, MSE and PSNR—A Comparative Study," *Journal of Computer and Communications*, vol. 7, no. 3, pp. 8–18, Mar. 2019, https://doi.org/10.4236/jcc.2019.73002.

[42] M. A. Al-Khasawneh and M. Mahmoud, "Safeguarding Identities with GAN-based Face Anonymization," *Engineering, Technology & Applied Science Research*, vol. 14, no. 4, pp. 15581–15589, Aug. 2024, https://doi.org/10.48084/etasr.7527.

[43] Z. Hossein-Nejad and M. Nasri, "An adaptive image registration method based on SIFT features and RANSAC transform," *Computers & Electrical Engineering*, vol. 62, pp. 524–537, Aug. 2017, https://doi.org/10.1016/j.compeleceng.2016.11.034.